Intense terahertz generation in two-color laser filamentation: energy scaling with terawatt laser systems

2013 New J. Phys. 15 075002

(http://iopscience.iop.org/1367-2630/15/7/075002)

New Journal of Physics
The open access journal for physics

Intense terahertz generation in two-color laser filamentation: energy scaling with terawatt laser systems

T I Oh, Y S You, N Jhajj, E W Rosenthal, H M Milchberg and K Y Kim[1]

Institute for Research in Electronics and Applied Physics, University of Maryland, Building 223, Paint Branch Drive, College Park, MD 20742, USA
E-mail: kykim@umd.edu

New Journal of Physics **15** (2013) 075002 (17pp)
Received 9 March 2013
Published 3 July 2013
Online at http://www.njp.org/
doi:10.1088/1367-2630/15/7/075002

Abstract. We investigate high-power terahertz (THz) generation in two-color laser filamentation using terawatt (TW) lasers including a 0.5 TW, 1 kHz system, as well as 2 and 30 TW systems both operating at 10 Hz. With these lasers, we study the macroscopic effect in filamentation that governs THz output energy yields and radiation profiles in the far field. We also characterize the radiation spectra at a broad range of frequencies covering radio–micro-waves to infrared frequencies. In particular, our 1 kHz THz source can provide high-energy ($>1\,\mu$J), high average power (>1 mW), intense ($>1\,\mathrm{MV\,cm^{-1}}$) and broadband (0.01–60 THz) THz radiation via two-color filamentation in air. Based on our scaling law, an ~30 TW laser can produce >0.1 mJ of THz radiation with multi-gigawatt peak power in ~1.5 m long filamentation.

[1] Author to whom any correspondence should be addressed.

Contents

1. Introduction

Strong terahertz (THz) pulse generation via ultrafast, two-color laser focusing in air has attracted considerable attention for broadband THz spectroscopy, THz imaging and nonlinear THz studies [1–25]. In this two-color scheme, an ultrashort laser's fundamental and its second harmonic pulses are focused in air (or any gas) to create a gaseous plasma via multiphoton/tunneling ionization. This emits a THz pulse in the forward direction. Compared to solid-state THz sources such as photoconduction in semiconductors [26, 27] or optical rectification in nonlinear crystals [28–31], two-color laser mixing provides intense, broadband THz pulses [15]. In particular, optical rectification in lithium niobate ($LiNbO_3$) crystals with tilted pulse front excitation provides extremely high THz energy (current record 125 μJ), but the radiation spectrum is mostly limited to <1.5 THz [31]. By contrast, two-color laser mixing is reported to provide ultra-broadband radiation up to 200 THz [15]. The source also produces extremely low-frequency radiation (<0.01 THz) [19]. Basically, this produces electromagnetic (EM) radiation ranging from radio-microwave to near-infrared frequencies. This provides an attractive characteristic for broadband spectroscopic studies.

Microscopically, THz radiation in two-color mixing originates from ultrafast plasma current generation during tunneling ionization [18–21], although there is still a debate on the mechanism. Besides this microscopic picture, equally important is the macroscopic laser-THz propagation effect. This is strongly coupled with femtosecond laser filamentation in air. In general, filamentation occurs due to dynamic balancing between Kerr-induced beam self-focusing and ionization-induced beam defocusing [32–34]. This results in a long filament ranging from a few centimeters to several meters depending on the laser and gas parameters. This filamentation naturally governs the macroscopic process of THz generation, making the two-color mixing phenomenon more complex. Practically, this macroscopic effect determines the far-field radiation profile [5, 23], polarization [24] and bandwidth [17], as well as THz energy scaling [19, 23].

Previously, an off-axis phase-matching mechanism was proposed and demonstrated to show this macroscopic effect in two-color filamentation [23]. We also showed that a long

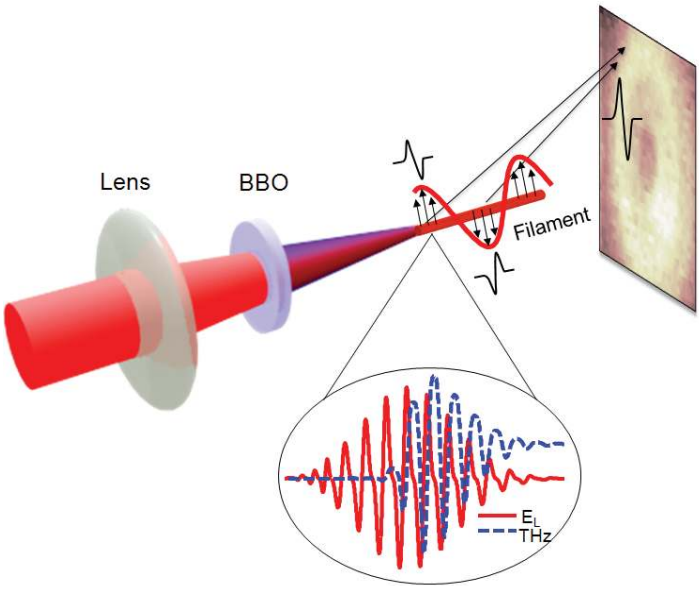

Figure 1. Schematic diagram of THz generation in two-color, femtosecond, laser filamentation in air. A microscopic plasma current (blue dotted line), produced by the two-color electric field (red solid line) via tunneling ionization, emits THz radiation in all directions. However, the far-field THz radiation profile shown on the detection plane is determined by macroscopic interference between the THz waves emitted from the local THz sources distributed along the filament. This provides an off-axis phase-matching condition, yielding conical THz radiation profiles. This macroscopic propagation effect also broadens the two-color laser and THz spectra via self-phase modulation and ionization-induced spectral blueshifts.

filament emits conical (donut-shaped) THz radiation peaked at 4–7° off from the forward axis depending on the radiation frequency. However, this phase-matching condition was demonstrated for relatively short filaments (<7 cm) with laser energy limited to <5 mJ [23]. In this paper, we extend the study for much longer filaments with multi-terawatt (TW) laser systems. In particular, we test THz energy scaling in long filamentation (1–60 cm) with 2 and 30 TW laser systems. Our scaling law predicts that the THz peak power can approach multi-gigawatt (GW) by creating about a meter long filament with a 30 TW laser system.

In parallel, we have investigated high average power THz generation at a 1 kHz repetition rate. For this, we have developed and used a cryogenically cooled Ti:sapphire amplifier capable of delivering 15 mJ per pulse at 1 kHz. This produces high average power (>1 mW) THz generation with >50 THz. Further enhancement toward 10 mW average power is also discussed. Finally, we address an issue associated with focusing conical THz radiation into a small spot size, which is of great importance for nearly all THz experiments.

2. Macroscopic model for terahertz (THz) generation in two-color filamentation

A schematic picture of two-color laser filamentation and simultaneous THz generation is shown in figure 1. A femtosecond laser pulse (ω) is weakly focused onto a frequency doubling crystal

such as beta barium borate (BBO), which generates a second harmonic pulse (2ω). In this in-line scheme, the BBO crystal is often detuned from its optimal angle (ω polarization parallel to the ordinary axis of the crystal) in order to produce an ω-field component parallel to 2ω polarized along the extraordinary axis. In this scheme, ω becomes elliptically polarized after passing through the crystal due to the birefringence in BBO [22]. Alternatively, the BBO crystal can be tuned at the right angle for type-I phase matching, which results in crossed polarization between ω and 2ω. This polarization state, however, can be converted into collinear by inserting a dichroic half-wave plate just after the BBO crystal (not shown in figure 1). In this way, the two-color laser fields can be linearly polarized in the same direction. Assuming this is the case, the laser field E_{L} at a point in the filament is expressed as

$$E_{\mathrm{L}} = E_{\omega}(t)\cos(\omega t) + E_{2\omega}(t)\cos(2\omega t + \theta), \tag{1}$$

where $E_{\omega}(t)$ and $E_{2\omega}(t)$ are the amplitudes of the fundamental and the second harmonic fields, respectively, and θ is the relative phase between $E_{\omega}(t)$ and $E_{2\omega}(t)$ at a distance d from the starting point of the filament. At the point, multiphoton/tunneling ionization occurs under the combined laser field and a plasma current arises from the tunnel-ionized electrons drifting in the combined laser field. Here, the local plasma current density is given by [20]

$$J(t) = -\int e v_{\mathrm{d}}(t, t')\,\mathrm{d}N_{\mathrm{e}}(t'), \tag{2}$$

where $\mathrm{d}N(t')$ is the density of free electrons produced by the laser field in the interval between t' and $t' + \mathrm{d}t'$, and $v_{\mathrm{d}}(t, t')$ is the drift velocity of those electrons at t. An ultrafast current surge at the point emits THz radiation in all directions, like dipole radiation from a point source, with the far-field scaling as $E_{\mathrm{THz}} \propto \mathrm{d}J(t)/\mathrm{d}t$. In the classical plasma current model, far-field THz radiation peaks at $\theta = \pm\pi/2$, while minimal THz radiation occurs at $\theta = 0$ [18]. The described plasma current model is also confirmed by numerical simulations [35].

The relative phase θ between the two-color laser fields, however, changes along the filament as

$$\theta = \omega(n_{\omega} - n_{2\omega})d/c + \theta_0, \tag{3}$$

where n_{ω} and $n_{2\omega}$ are the refractive indexes of the air–plasma filament at ω and 2ω frequencies, respectively, c is the speed of light in vacuum and θ_0 is the initial relative phase at the starting point of the filament. Here, the refractive index of the weakly ionized ($N_{\mathrm{e}} \ll N_{\mathrm{c}}$) air filament is given by $n_{\mathrm{filament}} = n_{\mathrm{air}} + \Delta n_{\mathrm{plasma}} + \Delta n_{\mathrm{Kerr}}$, where $\Delta n_{\mathrm{plasma}} \approx -\frac{1}{2}\,(N_{\mathrm{e}}/N_{\mathrm{c}})\,(1 + \mathrm{i}\nu/\omega)^{-1}$, N_{e} is the electron density, N_{c} is the critical density, and ν is the electron–ion collisional frequency that is negligible for the electron density of our interest ($\nu \ll \omega$). Because of this filament dispersion, the relative phase θ changes from 0 to π over a distance l_{d}, where $l_{\mathrm{d}} = (\lambda/2)\,(n_{\omega} - n_{2\omega})^{-1}$ is the dephasing length for ω and 2ω. Here, λ is the optical wavelength at ω. For pure (no plasma) atmospheric air ($\sim 10^{19}\,\mathrm{cm}^{-3}$), $l_{\mathrm{d}} = 25\,\mathrm{mm}$ at $\lambda = 800\,\mathrm{nm}$. For a filament with an electron density of $N_{\mathrm{e}} = 10^{16}\,\mathrm{cm}^{-3}$ in atmospheric air, $l_{\mathrm{d}} \approx 20\,\mathrm{mm}$. As this relative phase varies along the filament, the local THz amplitude and polarity also change along the filament as shown in figure 1 (see the red oscillating curve along the filament). Because of this oscillating THz source polarity, far-field THz radiation is not simply emitted in the forward direction [36].

In general, the THz far field, $E(r, \Omega)$, is obtained by integrating the contributions from all source points distributed along the filament as [23]

$$E(\mathbf{r}, \Omega) \propto \int_V \mathrm{d}^3\mathbf{r}' \frac{\tilde{P}\,(\mathbf{r}', \Omega)\;\mathrm{e}^{\mathrm{i}k_{\mathrm{THz}}|\mathbf{r}-\mathbf{r}'|}}{|\mathbf{r} - \mathbf{r}'|}, \tag{4}$$

where $\tilde{P}(\mathbf{r}', \Omega) \propto \tilde{A}(\mathbf{r}', \Omega) \sin(\theta(z')) \exp\left(\mathrm{i}n_g k_{\mathrm{THz}} z' - \mathrm{i}\Omega t\right)$is the nonlinear THz polarization, and $\tilde{A} \propto \mathrm{d}J(r', \Omega)/\mathrm{d}t$ is the local THz amplitude at frequency Ω, determined by the microscopic plasma current model [18–20]. At a distance far longer than the filament length ($|\mathbf{r} - \mathbf{r}'| \gg |\mathbf{r}'|$), the far-field THz intensity profile is approximated as [23]

$$|E(r, \Theta, \Omega)|^2 \propto |\tilde{A}(\boldsymbol{r}', \Omega)|^2 \frac{(\pi a^2)^2 l^2}{r^2} (\kappa_1^2 + \kappa_2^2 + 2\kappa_1 \kappa_2 \cos(2\theta_0 + \pi)) \left(\frac{2J_1(\beta)}{\beta}\right)^2, \tag{5}$$

where $\kappa_{1,2} = \sin(\alpha_{1,2})/\alpha_{1,2}$, $\alpha_{1,2} = k_{\mathrm{THz}} l[n_g \pm \Gamma/(2l_{\mathrm{d}}) - \cos(\Theta)]/2$, $\beta = 2\pi a \lambda^{-1} \sin(\Theta)$, Γ is the THz wavelength and the last term in equation (5) represents circular diffraction. The third term in equation (5) provides a phase-matching condition for efficient THz generation. Here, maximum THz generation is achieved with $\alpha_{1,2} = 0$. This provides the angle for phase matching, Θ_{p}, given by $\cos(\Theta_{\mathrm{p}}) = 1 - \Gamma/(2l_{\mathrm{d}})$ for weakly ionized plasma filaments ($n_g \approx 1$). The phase-matching angle Θ_{p} can also be obtained from the condition necessary for constructive interference between two oppositely polarized THz waves as shown in figure 1. This condition is satisfied when the path length difference becomes $\Gamma/2$, which provides the same phase-matching angle. For example, a filament length of $l = 70$ mm, 1 THz radiation ($\Gamma = 300\,\mu$m) peaks at $\Theta = 7^\circ$ with a conical radiation profile as shown in figure 1.

The total THz yield obtained from the entire filament length is given by $\int |E(r, \Theta, \Omega)|^2 \sin\Theta \, \mathrm{d}\Theta$. This scales quasi-linearly with the filament length [23]. This implies that we can enhance the output THz energy by increasing the filament length while maintaining the local THz strengths the same. This condition remains still valid for multi-filamentation. For example, two filaments separated by d (of the order of hundreds of micrometers) in the transverse direction would produce THz waves in phase and those two waves interfere destructively in the far field at an angle of $\theta_{\mathrm{d}} = \sin^{-1}(\Gamma/(2d))$. Compared with the phase-matching angle, $\Theta_{\mathrm{p}} = \cos^{-1}(1 - \Gamma/(2l_{\mathrm{d}}))$, θ_{d} at which destructive interference occurs due to multi-filamentation is much larger than the phase-matching angle Θ_{d} because $d \ll l_{\mathrm{d}}$. Thus multi-filamentation plays little or no role in determining the far-field THz radiation profile. The total plasma volume, however, will contribute to the output THz yield.

3. THz energy scaling with high-power laser systems

3.1. THz energy scaling with a 2 TW laser operating at 10 Hz

A 2 TW Ti:sapphire laser system capable of delivering ~3 cm of beam diameter, 800 nm, 100 mJ, 50 fs pulses, at a 10 Hz repetition rate is used for THz generation. The experimental setup is shown in figure 2(a). In addition to far-field THz measurements, a 5 mm diameter, single-loop wire (B-dot probe) is used to monitor the near-field, low-frequency THz waveforms. Basically, this can probe the local THz amplitudes and polarities. Previously, it was shown that the B-dot signal is strongly correlated with far-field THz radiation [19].

For B-dot measurements, ~50 mJ of laser energy is used to create >300 mm long filaments with $f = 2$ m focusing. A 0.1 mm thick BBO crystal (type-I) is placed in the beam path (~120 mm after the focusing lens) to generate collinear second harmonics. A B-dot probe is placed and scanned in the air plasma filament as shown in figure 2(a). A 0.5 GHz, 5 giga-sample/s oscilloscope is used to measure the induced voltage across the ends of the B-dot coil. According to Faraday's law, the induced voltage is given by $V = -\int \dot{\mathbf{B}} \cdot \mathbf{ds}$, where $\dot{\mathbf{B}}$ (B-dot) is the time derivative of the magnetic field, which arises from a transient current in the plasma

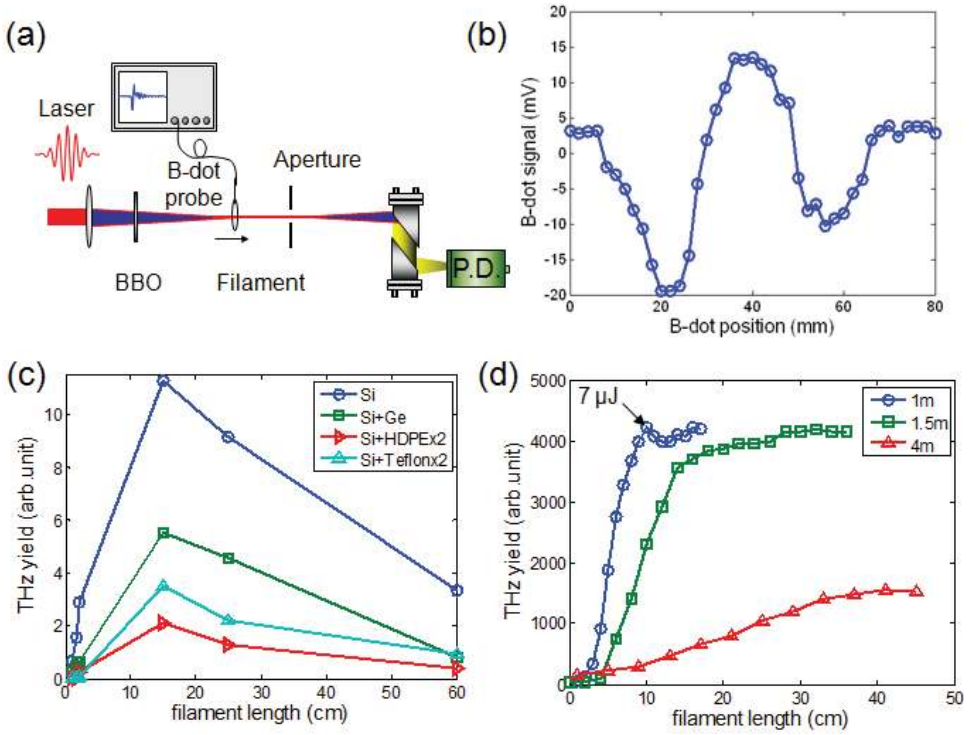

Figure 2. (a) Experimental setup for B-dot probe and THz energy measurements. (b) Peak-to-peak B-dot signal as a function of its position d along the plasma filament. (c) THz yield measured with a pyroelectric detector as a function of filament length made with six different focal length lenses. Four different transmission filters are used for THz detection at various bands (Si for <20 THz, Ge for <10 THz, HDPE or Teflon for 0.1–3 THz) [40]. For clarity, the yields for HDPE and Teflon are multiplied by a factor of 2. Here, the laser energy is fixed at 60 mJ. The maximum THz energy is 7 μJ obtained with ~10 cm long filamentation. (d) THz yield as a function of the iris position for three filaments produced by $f = 1$, 1.5 and 4 m focusing. Here the iris blocks THz radiation emitted before the aperture, which controls the effective filament length.

according to Ampere's law, $\nabla \times \dot{\mathbf{B}} = \mu_0 \dot{\mathbf{J}}$. Thus, the induced voltage (B-dot signal) represents the peak rate of electric current change where the probe is located [37]. Here we note that the plasma current, produced by detuned type-I phase matching, is generally elliptical [24]. This has a circular current component along the B-dot loop direction. To observe variations in the local plasma current with increasing filament length, the B-dot probe is scanned along the filament. As shown in figure 2(b), the B-dot signal (or local THz radiation) indeed oscillates with varying d (or θ) and the oscillation period is estimated to be $l_d \sim 20$ mm. This corresponds to an electron density of $N_e \sim 10^{16}$ cm^{-3}, consistent with other measurements [38, 39].

We also examine THz energy scaling and saturation in two-color filamentation with laser energy up to 60 mJ. In particular, we investigate laser energy coupling into filaments under various external focusing conditions. Figure 2(c) shows the output THz energy as a function of the filament length, varied from 1 to 60 cm with several focal lengths: $f = 15$, 20, 25, 100, 150 and 400 cm. Here the THz energy is measured with a pyroelectric detector with various

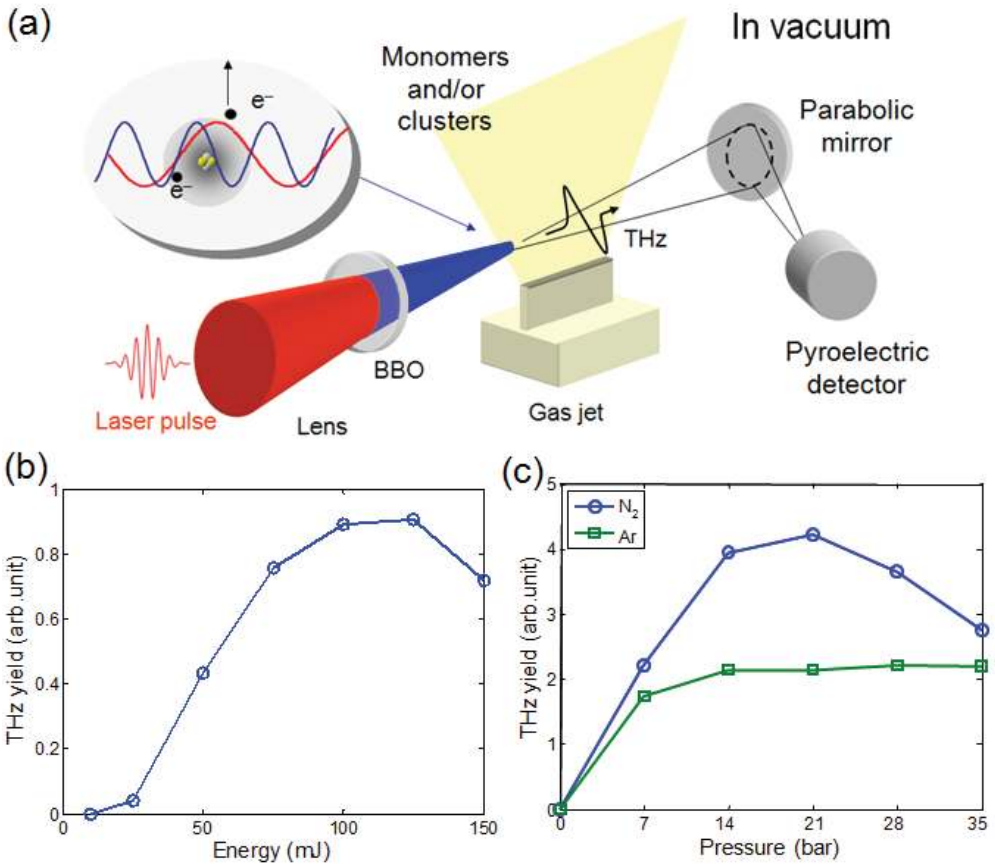

Figure 3. (a) Experimental setup for THz radiation from monomers and/or clusters ionized by a femtosecond two-color pulse in a vacuum chamber. Argon clusters are formed in an elongated gas jet via adiabatic expansion of high-pressure gas into vacuum. (b) THz yield from gaseous nitrogen jets as a function of laser energy at 14 bar backing pressure. (c) THz yields as a function of nitrogen gas and argon cluster targets with increasing backing gas pressure.

THz filters (Si, Ge, HDPE and Teflon). A silicon filter is used to block unwanted optical and infrared light. In addition to the Si filter, additional filters are used to characterize THz profiles at different frequency bands: a germanium wafer is used to detect THz frequencies mostly at $<$10 THz, whereas a 3 mm thick Teflon window is used as a low-pass filter to detect $<$3 THz. The yield increases with the filament length and peaks at 7 μJ with $f = 100$ cm focusing. With a focusing lens shorter than 100 cm, the input laser energy is not efficiently absorbed in creating a plasma filament, mainly due to strong ionization-induced defocusing [25]. This leads to laser intensity clamping in filamentation [32–34] and thus sets the maximum laser intensity for THz generation in air. On the other hand, when focused with a lens longer than 100 cm, the laser energy starts to spread out over the filament. This drops the local plasma-current amplitude, consequently yielding less THz radiation. This trend is consistent with the previous report [13].

We have also changed the effective filament length by scanning a pinhole aperture along the filament as shown in figure 2(a). The iris blocks the THz emitted before the aperture while not affecting the THz emitted after the aperture. Figure 2(d) shows the measured THz energy

as a function of the aperture position for filaments made with three focal length lenses ($f = 1$, 1.5 and 4 m). It shows that the total THz yield increases with the filament length, confirming off-axis phase matching up to ~50 cm long filamentation.

3.2. THz generation from gaseous and clustered plasma with a 30 TW, 10 Hz laser

We have also used a 30 TW (35 fs, 1 J) Ti:sapphire laser system for THz generation. Here we have conducted the experiment in a vacuum chamber (see figure 3(a)). In particular, we have tested gas/cluster jets for THz generation. An off-axis mirror (not shown) was used to focus incoming laser pulses onto elongated (~2 cm long) gas jets. Here, clusters—van der Waals-bonded aggregates of up to $\sim 10^7$ atoms—are formed in a condensing supersonic nozzle flow into vacuum [41]. In this experiment, two types of gas species, argon and nitrogen, are used. The emitted THz energy is collected by a parabolic mirror and focused into a pyroelectric detector. A silicon filter is placed in front of the detector.

Figure 3(b) shows THz output energy for nitrogen at 14 bar backing pressure and room temperature. The output yield increases with laser energy up to 100 mJ but soon drops after 100 mJ. This saturation is attributed to strong THz absorption in dense plasma [19] and/or plasma-induced laser defocusing in filamentation [25]. Here, the scaling test was limited to <200 mJ because of severe material damage and strong supercontinuum generation in the BBO substrate. Overall, the measured THz energy is much weaker than that obtained with the 2 TW laser in long filamentation. This is because the gas jet (or filament) length is limited to ~2 cm. Figure 3(c) shows THz yields as a function of gas backing pressure for nitrogen and argon. Both gases show strong saturations with increasing gas pressure, consistent with the previous reports [10, 19]. One interesting feature is that argon produces less THz energy compared to nitrogen. This contrasts the previous result performed for gas-phase targets [6, 19], where argon provides a higher THz yield compared to nitrogen. This is because the current argon jets produce much more and larger clusters compared to nitrogen in our experimental condition. This implies that clusters are not an efficient target for THz generation in two-color photoionization. Although a large fraction of laser energy up to 90% can be absorbed in a gas of clusters, the emitted THz radiation may be vastly absorbed by supercritical clustered plasmas.

3.3. High average power THz generation with a 0.5 TW, 15 mJ pulse^{-1}*, 1 kHz laser*

For high-peak and high-average-power THz generation, we have developed and used a cryogenically cooled Ti:sapphire amplifier. Figure 4(a) shows a photograph of our amplifier that delivers 800 nm, 15 mJ, 30 fs pulses at a 1 kHz repetition rate. A 6 mJ, ~150 ps (uncompressed) seed pulse from a commercial Ti:sapphire laser system (Legend Elite USX, Coherent Inc.) is amplified to 15 mJ in a 5 mm × 5 mm × 5.5 mm Ti:sapphire crystal pumped by a frequency-doubled (527 nm) Nd:YLF laser (Evolution HE, Coherent Inc.) providing 45 W at 1 kHz. To minimize thermal lensing in the gain medium caused by high-power pumping, the crystal rod is cooled down to ~60 K with a cryogenic refrigerator (PT-90, Cryomech Inc.). In order to avoid condensation at low temperature, the crystal rod is placed inside a vacuum chamber pumped down to 10^{-7}–10^{-8} Torr with a turbo pump (V-81M) backed up by a scroll pump (Varian, Agilent Technology Inc.). The amplification operates in the gain saturation regime for energy stability. This provides ~18 mJ uncompressed energy per pulse. We observe a small amount of spectral redshift in the amplification. This, in principle, can be improved by tilting the spectral

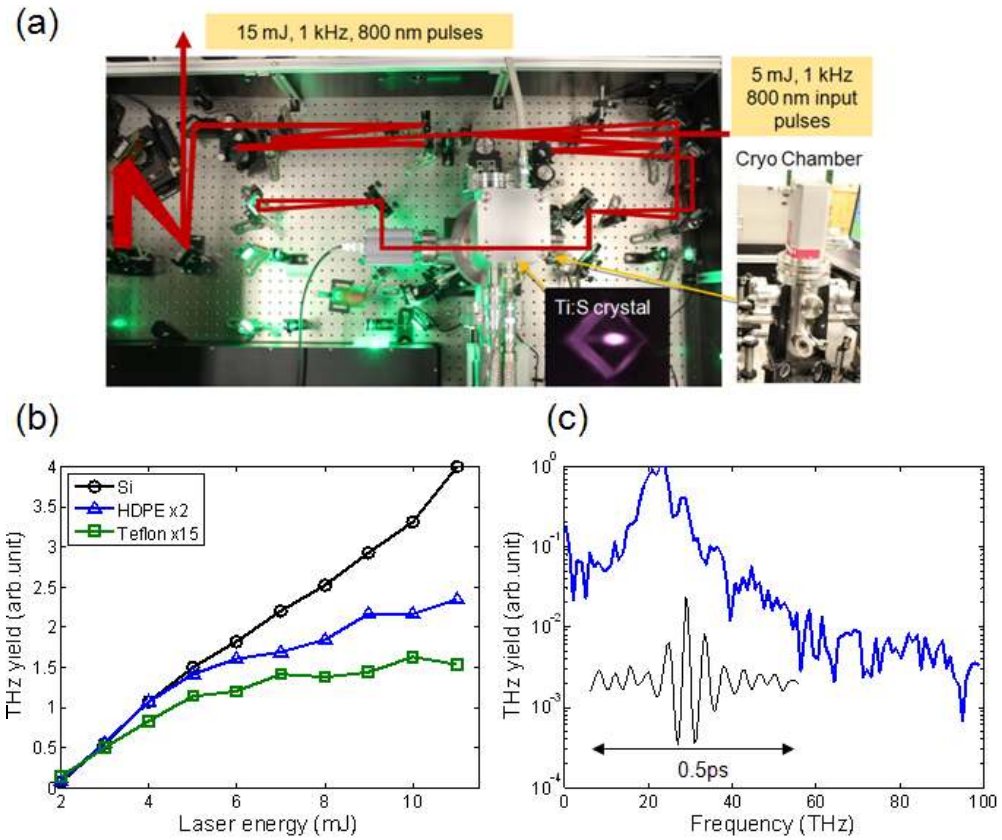

Figure 4. (a) Photography of a homebuilt cryogenically cooled Ti:sapphire amplifier capable of producing 15 mJ, 30 fs, 800 nm pulses at a 1 kHz repetition rate for high average power THz generation. (b) Measured THz output energy as a function of input laser energy with three different filter sets. For clarity, the yields for HDPE and Teflon are multiplied by a factor of 2 and 15, respectively. The maximum THz energy is $\sim$1 μJ pulse^{-1} at 1 kHz. (c) THz radiation spectrum measured by FTIR.

flattening filter in the regenerative amplifier and slightly blue-shifting the seed pulse. After amplification, the pulse duration is compressed back to <30 fs in a grating-based compressor with 84% transmission efficiency. This provides $\sim$0.5 TW peak power at 1 kHz.

Using the cryogenic amplifier system, we have generated THz radiation via two-color filamentation in air and tested THz energy scaling. The input laser energy is varied with a combination of a half-wave plate and a thin film polarizer. The THz pulse produced is collected and focused by a pair of off-axis parabolic mirrors into a pyroelectric detector (SPI-A-62THZ, Spectrum Detector Inc.).

Figure 4(b) shows measured THz output energy with increasing laser input energy. Three THz filters are used for detection at different frequency regions. The three lines in figure 4(b) show that the majority of radiation occurs at high frequencies. Note that the Teflon signal is rescaled by 15 times for clarity. In addition, the low-frequency radiation (<3 THz) saturates quickly whereas the high-frequency signal (Si filter) continues to increase with increasing input energy up to $\sim$11 mJ, providing THz energy of $\sim$1 μJ pulse^{-1}.

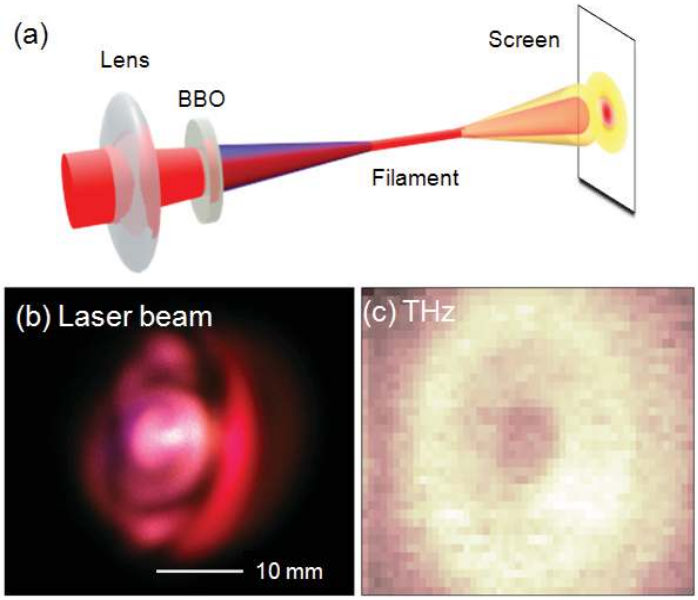

Figure 5. (a) Experimental setup for measuring THz far-field radiation profiles. The pyroelectric detector (not shown) is raster scanned over 3.5 cm × 5 cm on a screen at ∼20 cm away from the filament. (b) Two-color (800 and 400 nm) laser beam surrounded by a blue-shifted (600–700 nm) supercontinuum. (c) Measured THz profile. Here, both blue-shifted conical and THz radiation profiles are not symmetrical due to our imperfect beam condition.

Figure 4(c) shows a typical first-order interferometric field autocorrelation and the corresponding THz spectrum measured by Fourier transform infrared spectroscopy (FTIR) [19]. It shows radiation up to ∼60 THz with an input pulse duration of ∼30 fs. Even broader bandwidth ranging up to >100 THz is reportedly achieved by using a shorter (<20 fs) pulse duration [12, 15]. In our case, the majority of radiation occurs at high frequencies and peaks at 22 THz. This source is capable of providing 1 μJ pulse^{-1}, >60 THz pulses at 1 kHz and can be readily used for broadband nonlinear THz studies.

4. THz radiation profiles in long filamentation and refocusing

The previous section shows that high-energy THz radiation can be produced by an elongated filament which naturally forms a line source. Due to off-axis phase matching in filamentation, the line source emits conical THz radiation. In this section, we discuss such radiation profiles and in particular the issue of refocusing conical radiation into a small spot size.

Figure 5(a) shows an experimental layout for measuring a THz radiation profile in the far field. With $f = 1.5$ m focusing with 5 mJ laser energy, a >7 cm long filament is produced. A pyroelectric detector mounted on a two-dimensional (2D) motorized stage is raster scanned to measure the radiation profile. In addition, various THz transmission filters are placed to study high and low THz radiation profiles. Figure 5(b) shows the laser (800 and 400 nm) beam profile, surrounded by blue-shifted (600–700 nm) conical radiation, on a screen ∼20 cm away from the source filament. By contrast, the THz profile, obtained with a Teflon transmission filter, shows

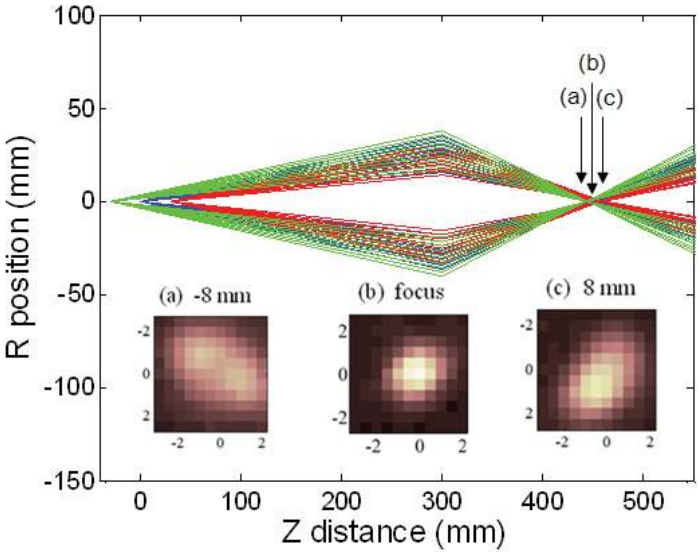

Figure 6. THz ray tracing calculation of an ∼7 cm long filament source and measured THz radiation profiles obtained (a) 8 mm before, (b) near and (c) 8 mm after the focal plane, all obtained with a 3 mm Teflon filter before the detector. Unlike the far-field profiles shown in figure 5, the focused radiation peaks on axis.

a donut-shaped structure. This off-axis radiation profile is attributed to the phase-matching condition in long filamentation [23]. Figure 5(c) shows an off-axis angle of 4–7° at 1–3 THz radiation, consistent with the theoretical phase-matching angle.

We also measure the profiles of THz radiation when refocused by a pair of parabolic mirrors. Figure 6 shows the radiation profiles obtained at three different axial positions: (a) 8 mm before, (b) at and (c) 8 mm after the focal plane, all with a 3 mm thick Teflon filter. The minimum spot size is ∼1.5 mm at 1–3 THz frequencies. Unlike the conical radiation shown in figure 5(c), the refocused THz intensity is peaked on axis (see figure 6(b)). This transition can be explained by ray tracing under geometric focusing as shown in figure 6. The refocused profile is bell-shaped, favorable for real applications, but the spot size inevitably increases with the filament length when the radiation from a line source is collected and focused by an off-axis parabolic mirror alone. In this case, the focused spot size scales as $D \sim l_{\mathrm{f}}\cos^{-1}[1 - \Gamma/(2l_{\mathrm{d}})]$, where l_{f} is the filament length and Γ is the THz wavelength. For an ∼7 cm long filament with $\Theta_{\mathrm{p}} \sim 5°$, the minimum spot size is calculated to be <1.5 mm, which agrees well with our measurements. This implies that THz energy benefits from long filamentation but not for THz refocusing. Ultimately, this affects the THz field strength at the focus. However, this refocusing problem can be corrected by collimating the far-field THz radiation with an axicon lens. More details are presented in section 6.

5. Ultra-broadband THz spectrum

Two-color photoionization can generate EM radiation at an extreme broad range covering RF to extreme ultraviolet (EUV). At first, an ultrafast photocurrent induced by two-color ionization creates EM radiation with a large bandwidth. Here the timescale for the current surge is much

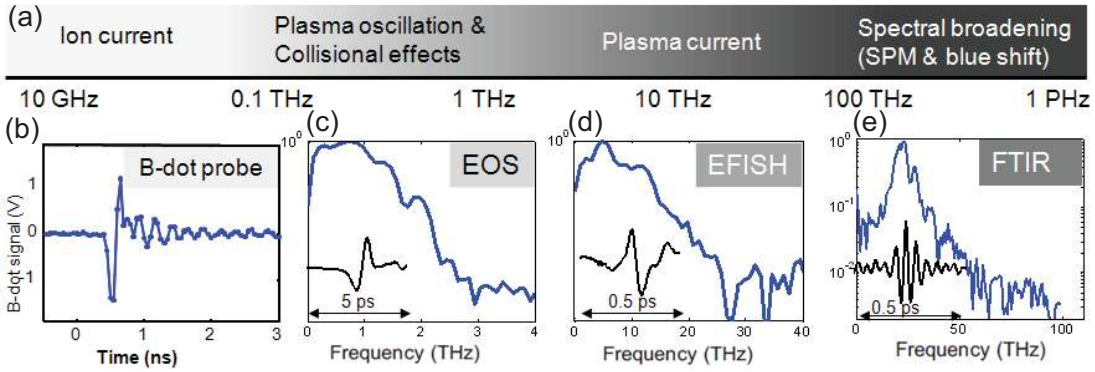

Figure 7. (a) Mechanisms for broadband EM radiation generation in two-color photoionization and radiation spectra measured with the (b) B-dot probe, (c) EOS in ZnTe, (d) EFISH and (e) FTIR techniques at broad frequency ranges.

shorter than the laser pulse duration because tunneling ionization occurs mostly around the peak intensity. For an ∼30 fs (FWHM) laser pulsewidth, for example, the total ionization process extends over as short as ∼12 fs (FWHM). This supports EM radiation with a bandwidth of >80 THz. This radiation bandwidth is further broadened and modulated by several mechanisms summarized in figure 7(a).

First, the laser spectrum broadens with propagation due to self-phase modulation in air, ionization-induced blueshifts and self-steepening. The broadened laser spectrum increases the THz bandwidth even further. The spectrum at 0.1–1 THz is strongly modulated by plasma oscillation and collisional effects. In addition, the plasma density of 10^{16}–10^{17} cm^{-3} strongly affects THz absorption in the filament direction. The collisional process ultimately terminates the plasma current. However, a very slow ion current can arise, producing radiation down to 0.01 THz. This corresponds to RF and micro-waves. At the other frequency end, broadband EUVs can be produced by optical high harmonic generation (HHG). In particular, two-color-based HHG can produce both odd and even harmonics, also enhancing the overall yields. This HHG is strongly connected with THz generation as they both arise from coherent motion of electrons in tunneling ionization [19, 42].

To detect such broadband radiation, various complementary methods must be applied. Figure 7 shows a list of our THz detection schemes along with measured radiation spectra. For example, the B-dot probe detects extremely low-frequency components such as RF and micro-waves. Figure 7(b) shows a sub-nanosecond electric current detected with a B-dot probe [19]. For THz detection at 0.1–3 THz, electro-optic sampling (EOS) with a 1 mm thick ZnTe crystal was adopted to measure THz waveforms (see figure 7(c)). The corresponding spectrum reaching up to 3 THz is obtained by a Fourier transform. Here, the detection bandwidth can be further increased by using a thinner and/or different EOS crystal having higher THz absorption lines, such as GaP.

Another method for broadband detection is using electric-field-induced second harmonic (EFISH), also known as air-biased coherent detection (ABCD) [14]. In this scheme, the THz pulse to be characterized is focused into air along with an ultrashort optical pulse, which produces an optical second harmonic by the EFISH effect. Here, the change in second harmonic yield is proportional to the THz electric field to be measured at the focus [14]. One big advantage

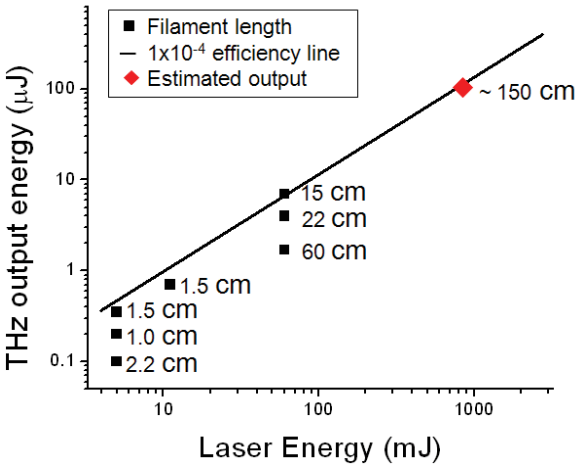

Figure 8. THz output energy as a function of input laser energy with various air filament lengths (black squares). The straight line represents maximum achievable THz energy with a conversion efficiency of 10^{-4}. An ~1.5 m long filament made with 1 J can yield ~100 μJ THz. The ultimate THz output energy is limited to ~300 μJ by the group velocity walk-off between two-color laser pulses. Here the fundamental laser wavelength is assumed to be 800 nm. We note that the optical to THz conversion efficiency can be further increased with longer wavelength (1–4 μm) pumping for filamentation [17, 43].

of this technique is its capability of detecting THz waveforms directly. However, the detection bandwidth is fundamentally limited by the probe pulse duration. Here, we have measured THz radiation up to 30 THz (see figure 7(d)), currently limited by our stretched probe pulsewidth (30–40 fs) and/or the size of the electrodes used for ABCD detection.

For even higher bandwidth detection, Michelson interferometry was used for FTIR [19]. Although FTIR does not directly provide THz waveforms, the detection bandwidth is not limited by the optical probe duration as in EFISH. Our measurement in figure 7(e) shows radiation up to 60 THz, largely limited by low laser energy usage in relatively short filamentation (see section 3.3).

6. Toward gigawatt peak-power THz generation

In this section, we discuss the outlook for high-peak-power THz generation and theoretical limits in two-color laser filamentation. Figure 8 summarizes THz energy scaling as a function of laser input energy. The black squares are our measurements obtained with various laser energy and filament length conditions. For a given laser energy, there is a favorable filament length that yields the optimal THz conversion efficiency, 10^{-4}. This is represented as the straight line in figure 8.

For instance, a 10 mJ laser input energy will yield ~1 μJ THz energy with an optimal filament length of ~2 cm. A 100 mJ laser energy will require a >15 cm long filament to produce ~10 μJ THz energy. An input of 1 J laser energy, readily available with our 30 TW laser system, will yield 100 μJ of THz energy with an estimated filament length of ~1.5 m (red diamond in the figure). The corresponding peak power will approach multi-GW with a 100 THz bandwidth.

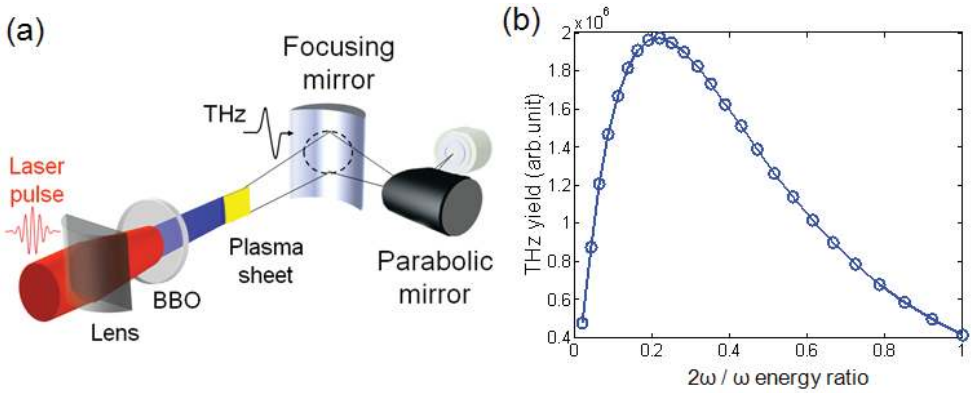

Figure 9. (a) Proposed experimental setup for scalable THz generation in a 2D plasma sheet using cylindrical lens focusing and recollection. (b) Simulated THz output energy as a function of the energy ratio of 2ω to ω with the total energy fixed. The output peaks at ratio ≈ 0.2 according to the microscopic plasma current model [18].

The maximum achievable THz energy, however, is limited by the group velocity walk-off between two-color laser pulses. Due to air–plasma dispersion, two 50 fs pulses at 800 and 400 nm, for example, get separated in time as they propagate over ~4 m in air [23]. This can produce ~300 μJ THz energy, a theoretical limit in two-color filamentation in air if the walk-off is not compensated.

Long filaments require a large parabolic mirror for THz energy collection. In addition, THz refocusing is another issue as discussed before. One method in reducing the filament length while keeping the same high-energy THz output is to increase the plasma filament volume in the transverse direction. Focusing two-color laser pulses with a cylindrical lens can create a plasma sheet as shown in figure 9(a). For a laser input of 1 J, a plasma sheet of ~1 cm^2 can be created. For THz collection and refocusing, a combination of a cylindrical mirror and a parabolic mirror can be used for tighter focusing.

For further THz energy scaling, the intensity of second harmonics needs to be increased. For example, figure 9(b) shows a simulation result of THz output as a function of the ratio of the second harmonic intensity to the fundamental intensity, $I_{2\omega}/I_{\omega}$. According to the microscopic plasma current model, the output THz yield peaks at $I_{2\omega}/I_{\omega} \approx 20\%$ with $I_{2\omega} = 2 \times 10^{13}$ W cm^{-2}. In our experiments, the ratio is typically ~8%. This is partly because the frequency doubling crystal (BBO) is intentionally detuned from its optical angle. This scheme can be improved by using an ultrathin, dichroic half-wave plate right after the BBO crystal [16]. This allows us to optimize not only the efficiency in second harmonic generation with type-I phase matching but also the amplitude of plasma current at the focus. Also the ultrathin thickness minimizes the two-color walk-off and pulse stretching. In addition, more efficient crystals such as BIBO [44] can be used to increase the conversion efficiency toward 20%.

Finally, a gas cell can be used for further THz enhancement. Previous results show that gases with low ionization potential such as krypton or xenon can dramatically increase THz output energy [6, 10, 19]. However, as those gases can easily saturate the output signal, it is important to increase the filament length accordingly. Combined with the ultrathin wave plate technique, this can increase the conversion efficiency toward 10^{-3}. For better refocusing,

a conical lens (axicon) made of silicon or an axicon mirror can be used to collimate the conical THz emission. Here we note that THz generation with axicon-based laser focusing was previously discussed [45, 46], but our scheme proposes using an axicon for THz beam collimation only, not for laser beam focusing as in [45, 46]. After collimation, a conventional off-axis parabolic mirror can be used for diffraction-limited refocusing. With our 1 kHz Ti:sapphire system capable of delivering 15 mJ pulse^{-1}, this gas cell method will produce 10 μJ pulse^{-1} at 1 kHz, corresponding to 10 mW average power, with a potential bandwidth of 100 THz. With an assumption of 100 fs THz pulse duration, the corresponding electric field at the focus will be 3 MV cm^{-1} with uncompensated refocusing ($\sim$1 mm diameter), while it will approach 100 MV cm^{-1} with diffraction-limited focusing (30 μm diameter). This source will be a very useful tool in high-power THz studies, including broadband nonlinear spectroscopy and imaging applications.

7. Conclusion

In summary, we have discussed intense THz generation and its theoretical limit in two-color laser filamentation, with an emphasis on the macroscopic propagation effect. Experimentally, we have used three TW laser systems (0.5, 2 and 30 TW) to create a broad range of filament conditions. Our simulation and experimental results confirm scalable THz generation with increasing filament length, as well as ultra-broadband EM radiation generation covering RF–micro-waves to near-infrared frequencies.

With our 2 TW system, we have produced $\sim$7 μJ of THz energy with a 15 cm long filament at 10 Hz. Further enhancement to 100 μJ can be achievable in 1.5 m long filamentation by using a 30 TW laser. This can provide multi-GW peak power with a 100 THz bandwidth. In terms of high average power, our kHz system can currently provide 1 mW with $\sim$1 μJ pulse^{-1}. The focused field strength is $>$1 MV cm^{-1} but can be enhanced up to $\sim$100 MV cm^{-1} with ionization in a gas cell and axicon-based beam collimation. Due to this broadband and high-field strength, two-color laser filamentation will be a very useful source for research in broadband THz spectroscopy and strong THz field studies.

Acknowledgments

We acknowledge the support of the US Department of Energy and the Office of Naval Research. We also thank Sanjay Varma, Yu-Hsin Chen and Brian Layer for their contributions in operating the laser systems and conducting partial experimental tasks.

References

[1] Cook D J and Hochstrasser R M 2000 Intense terahertz pulses by four-wave rectification in air *Opt. Lett.* **25** 1210–2

[2] Kress M, Löffler T, Eden S, Thomson M and Roskos H G 2004 Terahertz-pulse generation by photoionization of air with laser pulses composed of both fundamental and second-harmonic waves *Opt. Lett.* **29** 1120–2

[3] Bartel T, Gaal P, Reimann K, Woerner M and Elsaesser T 2005 Generation of single-cycle THz transients with high electric-field amplitudes *Opt. Lett.* **30** 2805–7

[4] Xie X, Dai J and Zhang X-C 2006 Coherent control of THz wave generation in ambient air *Phys. Rev. Lett.* **96** 075005

[5] Zhong H, Karpowicz N and Zhang X-C 2006 Terahertz emission profile from laser-induced air plasma *Appl. Phys. Lett.* **88** 261103
[6] Chen Y, Yamaguchi M, Wang M and Zhang X-C 2007 Terahertz pulse generation from noble gases *Appl. Phys. Lett.* **91** 251116
[7] Dai J, Karpowicz N and Zhang X-C 2009 Coherent polarization control of terahertz waves generated from two-color laser-induced gas plasma *Phys. Rev. Lett.* **103** 023001
[8] Wen H and Lindenberg A M 2009 Coherent terahertz polarization control through manipulation of electron trajectories *Phys. Rev. Lett.* **103** 023902
[9] Blanchard F, Sharma G, Ropagnol X, Razzari L, Morandotti R and Ozaki T 2009 Improved terahertz two-color plasma sources pumped by high intensity laser beam *Opt. Express* **17** 6044–52
[10] Rodriguez G and Dakovski G L 2010 Scaling behavior of ultrafast two-color terahertz generation in plasma gas targets: energy and pressure dependence *Opt. Express* **18** 15130–43
[11] Wang T-J, Daigle J-F, Chen Y, Marceau C, Théberge F, Châteauneuf M, Dubois J and Chin S L 2010 High energy THz generation from meter-long two-color filaments in air *Laser Phys. Lett.* **7** 517–21
[12] Thomson M D, Blank V and Roskos H G 2010 Terahertz white-light pulses from an air plasma photo-induced by incommensurate two-color optical fields *Opt. Express* **18** 23173
[13] Wang T-J, Marceau C, Yuan S, Chen Y, Wang Q, Théberge F, Châteauneuf M, Dubois J and Chin S L 2011 External focusing effect on terahertz emission from a two-color femtosecond laser-induced filament in air *Laser Phys. Lett.* **8** 57–61
[14] Dai J, Clough B, Ho I-C, Lu X F, Liu J and Zhang X-C 2011 Recent progresses in terahertz wave air photonics *IEEE Trans. Terahertz Sci. Technol.* **1** 274–81
[15] Matsubara E, Nagai M and Ashida M 2012 Ultrabroadband coherent electric field from far infrared to 200 THz using air plasma induced by 10 fs pulses *Appl. Phys. Lett.* **101** 011105
[16] Minami Y, Kurihara T, Yamaguchi K, Nakajima M and Suemoto T 2013 High-power THz wave generation in plasma induced by polarization adjusted two-color laser pulses *Appl. Phys. Lett.* **102** 041105
[17] Bergé L, Skupin S, Köhler C, Babushkin I and Herrmann J 2013 3D numerical simulations of THz generation by two-color laser filaments *Phys. Rev. Lett.* **110** 073901
[18] Kim K-Y, Glownia J H, Taylor A J and Rodriguez G 2007 Terahertz emission from ultrafast ionizing air in symmetry-broken laser fields *Opt. Express* **15** 4577–84
[19] Kim K-Y, Taylor A J, Glownia J H and Rodriguez G 2008 Coherent control of terahertz supercontinuum generation in ultrafast laser–gas interactions *Nature Photon.* **2** 605–9
[20] Kim K-Y 2009 Generation of coherent terahertz radiation in ultrafast laser–gas interactions *Phys. Plasmas* **16** 056706
[21] Kim K-Y, Glownia J H, Taylor A J and Rodriguez G 2012 High-power broadband terahertz generation via two-color photoionization in gases *IEEE J. Quantum Electron.* **48** 797–805
[22] Oh T I, You Y S and Kim K-Y 2012 Two-dimensional plasma current and optimized terahertz generation in two-color photoionization *Opt. Express* **20** 19778–86
[23] You Y S, Oh T I and Kim K-Y 2012 Off-axis phase-matched terahertz emission from two-color laser-induced plasma filaments *Phys. Rev. Lett.* **109** 183902
[24] You Y S, Oh T I and Kim K-Y 2013 A mechanism of elliptically polarized terahertz generation in two-color laser filamentation *Opt. Lett.* **38** 1034–6
[25] Oh T I, You Y S, Jhajj N, Rosenthal E W, Milchberg H M and Kim K-Y 2013 Scaling and saturation of high-power terahertz radiation generation in two-color laser filamentation *Appl. Phys. Lett.* **102** 201113
[26] You D, Jones R R, Bucksbaum P H and Dykaar D R 1993 Generation of high-power sub-single-cycle 500-fs electromagnetic pulses *Opt. Lett.* **18** 290–2
[27] Dreyhaupt A, Winnerl S, Dekorsy T and Helm M 2005 High-intensity terahertz radiation from a microstructured large-area photoconductor *Appl. Phys. Lett.* **86** 121114
[28] Yeh K-L, Hoffmann M C, Hebling J and Nelson K A 2007 Generation of 10 μJ ultrashort terahertz pulses by optical rectification *Appl. Phys. Lett.* **90** 171121

[29] Blanchard F *et al* 2007 Generation of 1.5 μJ single-cycle terahertz pulses by optical rectification from a large aperture ZnTe crystal *Opt. Express* **15** 13212–20
[30] Stepanov A G, Bonacina L, Chekalin S V and Wolf J-P 2008 Generation of 30 μJ single-cycle terahertz pulses at 100 Hz repetition rate by optical rectification *Opt. Lett.* **33** 2497–9
[31] Fülöp J A, Pálfalvi L, Klingebiel S, Almási G, Krausz F, Karsch S and Hebling J 2012 Generation of sub-mJ terahertz pulses by optical rectification *Opt. Lett.* **37** 557–9
[32] Couairon A and Mysyrowicz A 2007 Femtosecond filamentation in transparent media *Phys. Rep.* **441** 47–189
[33] Chin S L *et al* 2012 Advances in intense femtosecond laser filamentation in air *Laser Phys.* **22** 1–53
[34] Bergé L, Skupin S, Nuter R, Kasparian J and Wolf J-P 2008 Ultrashort filaments of light in weakly ionized, optically transparent media *Rep. Prog. Phys.* **71** 109801
[35] Babushkin I, Skupin S, Husakou A, Köhler C, Cabrera-Granado E, Bergé L and Herrmann J 2011 Tailoring terahertz radiation by controlling tunnel photoionization events in gases *New J. Phys.* **13** 123029
[36] Köhler C, Cabrera-Granado E, Babushkin I, Bergé L, Herrmann J and Skupin S 2011 Directionality of terahertz emission from photoinduced gas plasmas *Opt. Lett.* **36** 3166–8
[37] Hosseini S A, Ferland B and Chin S L 2003 Measurement of filament length generated by an intense femtosecond laser pulse using electromagnetic radiation detection *Appl. Phys.* B **76** 583–6
[38] Chen Y-H, Varma S, Antonsen T M and Milchberg H M 2010 Direct measurement of the electron density of extended femtosecond laser pulse-induced filaments *Phys. Rev. Lett.* **105** 215005
[39] Rodriguez G, Valenzuela A R, Yellampalle B, Schmitt M J and Kim K-Y 2008 In-line holographic imaging and electron density extraction of ultrafast ionized air filaments *J. Opt. Soc. Am.* B **25** 1988–97
[40] Lee Y-S 2008 *Principles of Terahertz Science and Technology* (New York: Springer)
[41] Kim K Y, Kumarappan V and Milchberg H M 2003 Measurement of the average size and density of clusters in a gas jet *Appl. Phys. Lett.* **83** 3210–12
[42] Zhang D, Lü Z, Meng C, Du X, Zhou Z, Zhao Z and Yuan J 2012 Synchronizing terahertz wave generation with attosecond bursts *Phys. Rev. Lett.* **109** 243002
[43] Wang W-M, Kawata S, Sheng Z-M, Li Y-T, Chen L-M, Qian L-J and Zhang J 2011 Efficient terahertz emission by mid-infrared laser pulses from gas targets *Opt. Lett.* **36** 2608–10
[44] Harimoto T, Takeuchi Y and Fujita M 2004 Spectral properties of second-harmonic generation at 800 nm in a BiB_3O_6 crystal *Opt. Express* **12** 811–6
[45] Gildenburg V B and Vvedenskii N V 2007 Optical-to-THz wave conversion via excitation of plasma oscillations in the tunneling-ionization process *Phys. Rev. Lett.* **98** 245002
[46] Manceau J-M, Averchi A, Bonaretti F, Faccio D, Di Trapani P, Couairon A and Tzortzakis S 2009 Terahertz pulse emission optimization from tailored femtosecond laser pulse filamentation in air *Opt. Lett.* **34** 2165–7